Part II

Non-destructive measurements

The particles emitted in a collision, Fig. I.1, have position, momentum, charge, and other properties (e.g. lifetime) which we wish to measure. If the interaction with a detecting medium transfers but little energy to that medium, the measurement is called non-destructive. Within this category we distinguish between measurements of time and velocity (Chapters 2–4) and measurements using ionization (Chapter 6) but limited by scattering (Chapter 5) of the trajectory of the particles in the detecting medium (Chapters 7–9).

In the first case physical processes which depend on velocity are used, while in the latter the trajectory in electric and magnetic fields is used (Chapters 7–9) to infer the position, momentum, and charge of a particle.

Part IIA

Time and velocity

In Chapter 2, we examine the photoelectric effect whereby light is converted to an electrical signal. Devices using this effect are commonplace; for example photocells which are used to control the doors of elevators. By utilizing photomultiplier tubes and scintillating materials, precise time measurements can be made. These 'clocks' are then used to measure velocity as the time to go to a fixed distance. In Chapter 3 we turn to the Cerenkov radiation which is emitted at a velocity dependent angle when a charged particle moves with a velocity which exceeds the velocity of light in a medium. The emitted light can be converted to an electrical signal using the techniques of Chapter 2. Chapter 4 concerns x-ray radiation emitted by a charged particle in a medium with index of refraction <1. This 'sub-threshold' Cerenkov photon emission is used to measure particles moving at velocities very near to the speed of light.

2

The photoelectric effect, photomultipliers, scintillators

There is a crack in everything, that's how the light gets in.
Leonard Cohen

Time is nature's way of keeping everything from happening at once.
Anon

Of the physical scattering processes introduced in Chapter 1, the photoelectric effect is our starting point. The effect is due to the absorption of a photon by an atom with subsequent electron emission. We first derive the photoelectric cross section and examine the regime (low photon energy) where it dominates. This chapter then takes up our first extended discussion of a detector, the photomultiplier tube. Applications of the device include time of flight measurements with fast scintillators, and coincidence logic. A discussion of light collection in scintillation counters explores both classical 'light pipes' and 'wavelength shifting' techniques. Other devices also require a knowledge of the photoelectric effect. For example see Chapter 4 where the transition radiation detector performance depends critically on photoelectric absorption of the emitted x-rays.

2.1 Interaction Hamiltonian

As we saw from the data shown in Chapter 1, the low energy interaction of a photon is dominated by the photoelectric effect. This effect was first explained quantitatively by Einstein, using the new quantum theory and treating the photon as a particle. A schematic of the process in which there is an incident plane wave with wave number k, wavelength λ, and frequency ω, is shown in Fig. 2.1. Also indicated is the energy level diagram appropriate to the kinematics. The atom is initially in a bound state with negative energy $-\varepsilon$ and is described by a wave function $u_0(r)$. The final state for the electron has momentum p and exists in the ionization continuum as a free particle.

The free particle Hamiltonian H_0, is modified in the presence of an electromagnetic field by an interaction term arising from a replacement of the momentum, $\mathbf{p} \rightarrow \mathbf{p} - ie\mathbf{A}$ where $\mathbf{A}$ is the vector potential of the electromagnetic field. This replacement is valid in both classical mechanics and quantum

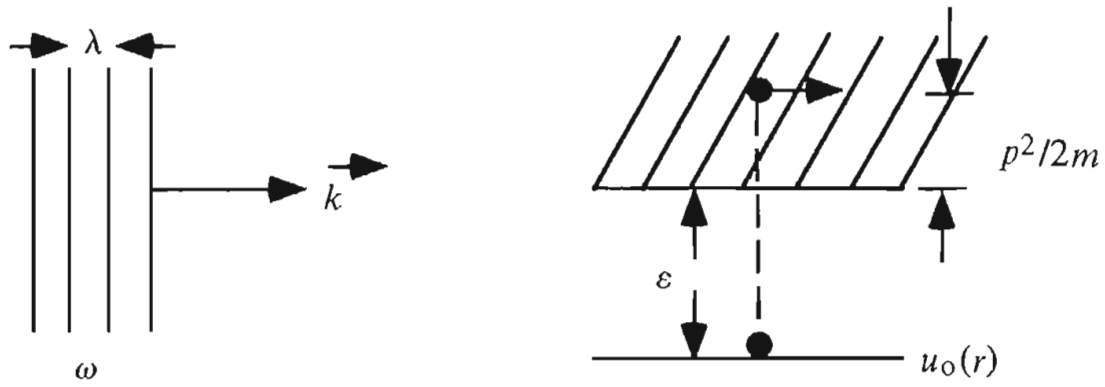

Fig. 2.1. Energy level diagram for the kinematics of the photoelectric effect.

mechanics. It leads to an interaction term in the Hamiltonian, H_I, which is proportional to the vector potential, **A**, of the photon and the momentum **p** of the electron.

$$\begin{aligned} H_0 &= p^2/2m \\ \mathbf{p} &\rightarrow \mathbf{p} - ie\mathbf{A} \\ H_I &\sim \left(\frac{ie\mathbf{p}\cdot\mathbf{A}}{m}\right) \end{aligned} \tag{2.1}$$

The kinematics for classical energy and momentum conservation are

$$\begin{aligned} -\varepsilon + \hbar\omega &= p^2/2\mathrm{m} \\ \mathbf{p}_e + \hbar\mathbf{k} &= \mathbf{p} \end{aligned} \tag{2.2}$$

Ignoring the small energy of the recoil atom, the final state energy is simply the kinetic energy of the ionized electron. The wave vector **k** refers to the initial photon state, while **p** refers to the final state free electron. The initial electron momentum $\mathbf{p}_e$ is not observed. Therefore this free variable is 'integrated over' in the sense that the initial state wave function, $u_o(r)$, contains the probability to obtain different initial electron momenta.

2.2 Transition amplitude and cross section

In non-relativistic perturbation theory the lowest order transition amplitude is the matrix element, A, of the interaction potential between the unperturbed initial and final states.

$$\begin{aligned} A &= \langle f|H_1|i\rangle \\ &\sim \frac{e}{m}\int e^{i\mathbf{p}\cdot\mathbf{r}/\hbar}(\mathbf{A}\cdot\mathbf{p})u_0(r)d\mathbf{r} \end{aligned} \tag{2.3}$$

Details of the calculation are given in Appendix C. Here we simply sketch the steps.

We need an expression for the bound state wave function of the inner shell electrons in the lowest angular momentum state. Recall that the square of the wave function is the probability density. Since the characteristic size for the state is the Bohr radius, a, the wave function is contained in a volume $<\pi a^3$ or $|u_0(r)|^2 \sim 1/\pi a^3$. Referring to Appendices B and C, the bound state wave function is:

$$u_0(r) \sim \frac{1}{\sqrt{\pi a^3}} e^{-r/a}$$
$$a_0 = \lambda\!\!\!^{-}/\alpha, \quad a \sim a_0/Z \tag{2.4}$$

The inner electrons in an atom 'see' the full charge, Z, of the nucleus unscreened by the other electrons and thus are bound tightly. Therefore, their radius is reduced with respect to the hydrogenic Bohr radius by a factor $1/Z$.

The matrix element A is proportional to $(\lambda_{DB}/a)^4$ where λ_{DB} is the outgoing electron de Broglie wavelength $\lambda_{DB} \equiv \hbar/p$. The smallness of the amplitude is due to the poor overlap integral for A since $a \gg \lambda_{DB}$. Basically, it is very unlikely to find a high momentum in the initial state. Thus the photoelectric cross section, σ_{PE}, scales in a complicated way with photon energy. The main physics contribution is the $(\lambda_{DB}/a)^8 = (\hbar/pa)^8$ behavior coming from the square of the matrix element. As before, $\lambda\!\!\!^{-}$ is the Compton wavelength of the electron.

$$\sigma_{PE} \sim \alpha \lambda\!\!\!^{-2} \left[\frac{mc^2}{\hbar\omega}\right] [\lambda_{DB}/a]^5$$
$$\sim 1/\omega^{7/2} \tag{2.5}$$
$$\hbar\omega \sim p^2/2m \quad \text{(Eq. 2.2)}$$

The cross section falls rapidly with incident photon energy; in this approximation as $1/\omega^{7/2}$. Therefore the photoelectric effect is only important at low photon energies as is, indeed, clear looking back at Chapter 1.

If the photon has an energy which is equal to the energy of one of the inner electrons, an enhanced absorption will occur. The simple approximate generalization of the Bohr result for different principle quantum numbers, n, and for inner electrons bound to atoms with atomic number Z is given below. The effect for E_n is taken care of by the replacement $U = e^2/r \rightarrow U = (Ze)(e)/r$ or $\alpha \rightarrow Z\alpha$.

$$E_n = -\left[\frac{mc^2}{2}(Z\alpha)^2\right]/n^2$$
$$= -13.6eV\,[Z^2/n^2] \tag{2.6}$$

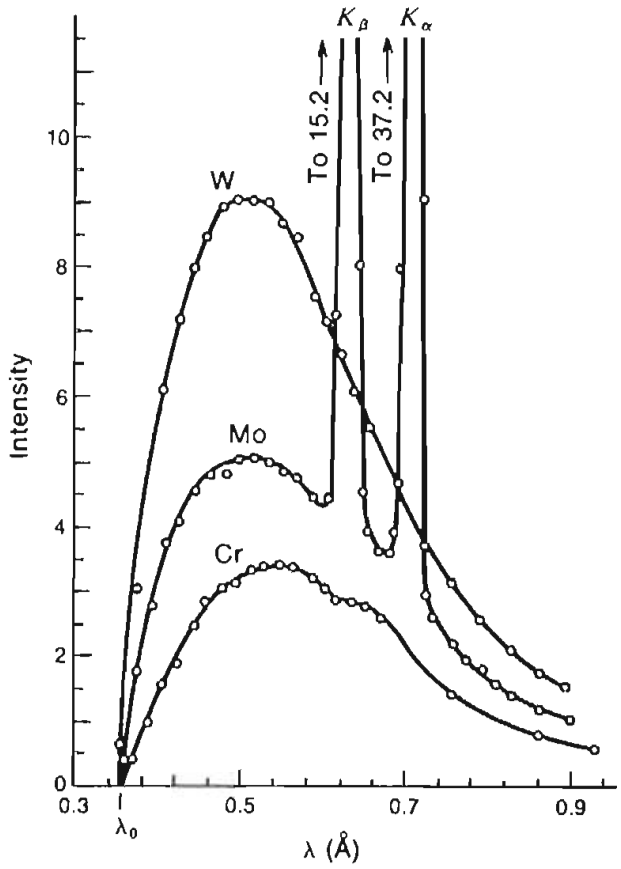

Fig. 2.2. Data on the intensity of emitted x-rays as a function of wavelength in various heavy elements. The 'quantized' lines corresponding to the binding energies of the inner electrons are very evident. (From Ref. 1.7, with permission.)

Some representative data on the intensity of the emitted x-ray for the inverse process in various heavy elements is shown in Fig. 2.2. In this inverse process, $e + A \rightarrow \gamma + A^*$, elements under electron bombardment emit x-ray photons. The photon emission occurs when the atom, A*, de-excites by an inner electron transition accompanied by the emission of an x-ray with a quantized wave length. The scale for λ is Å, or keV energies, as expected from Eq. 2.6.

Data on the relationship between the square root of the emitted frequency and the atomic number is shown in Fig. 2.3. As expected from Eq. 2.6, the bound state energies, and therefore the emitted x-ray frequencies are proportional to Z^2, which is called Moseley's law. The mechanism of x-ray emission by electron bombardment is the basis of medical and dental radiology and is now a commonplace.

The inverse mean free path, in $(g/cm^2)^{-1}$, as a function of the photon energy incident on lead is shown in Fig. 2.4. We calculate the inner electron binding energy for lead for the first two principle quantum numbers. The computed energies from Eq. 2.6 are 91 and 23 keV respectively. As seen in Fig. 2.4, there is pronounced structure at an incident photon energy corresponding to these

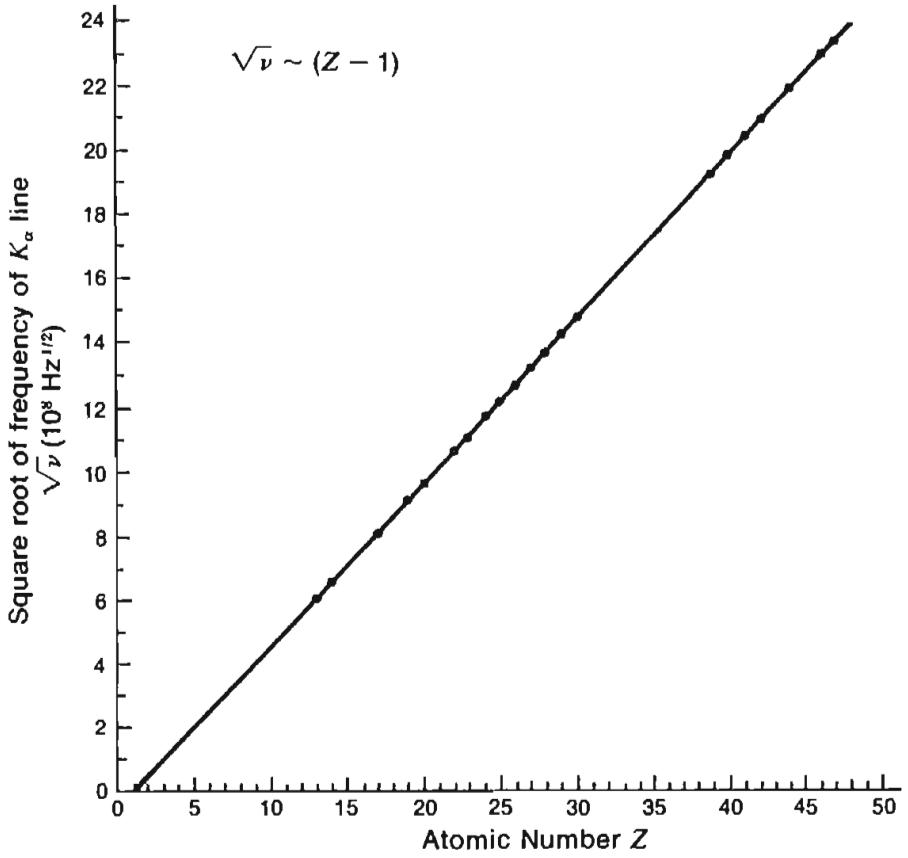

Fig. 2.3. Data on the relationship between the x-ray wavelength and the atomic number. The $\hbar\omega = E \sim Z^2$ behavior expected from Eq. 2.6 is observed. (From Ref. 1.7, with permission.)

two energies. We compare the photoelectric cross section to the Thomson cross section, σ_T, for photon elastic scattering off free electrons given in Table 1.1 and derived later in Chapter 10. Assuming that Thomson scattering is incoherent, the sum over Z electrons is simply Z times the cross section off a single electron.

$$\sigma_{PE} \sim \frac{32\pi}{3}\sqrt{2}(Z\alpha)^4 Z\left(\frac{m}{\hbar\omega}\right)^{7/2}(\alpha\lambda\!\!\!^{-})^2$$

$$\sigma_T \sim \frac{8\pi}{3}Z(\alpha\lambda\!\!\!^{-})^2 \tag{2.7}$$

$$\sigma_{PE}/\sigma_T \sim 4\sqrt{2}(Z\alpha)^4(m_e c^2/\hbar\omega)^{7/2}$$

Therefore, for heavy atoms where $Za \sim 1$, we expect the photoelectric effect to dominate over Thomson scattering for energies, $\hbar\omega < mc^2 \sim 0.51$ MeV. Indeed, this is the observed behavior and the approximate energy region where the two cross sections are comparable. For example, in lead, a photon with 10 keV

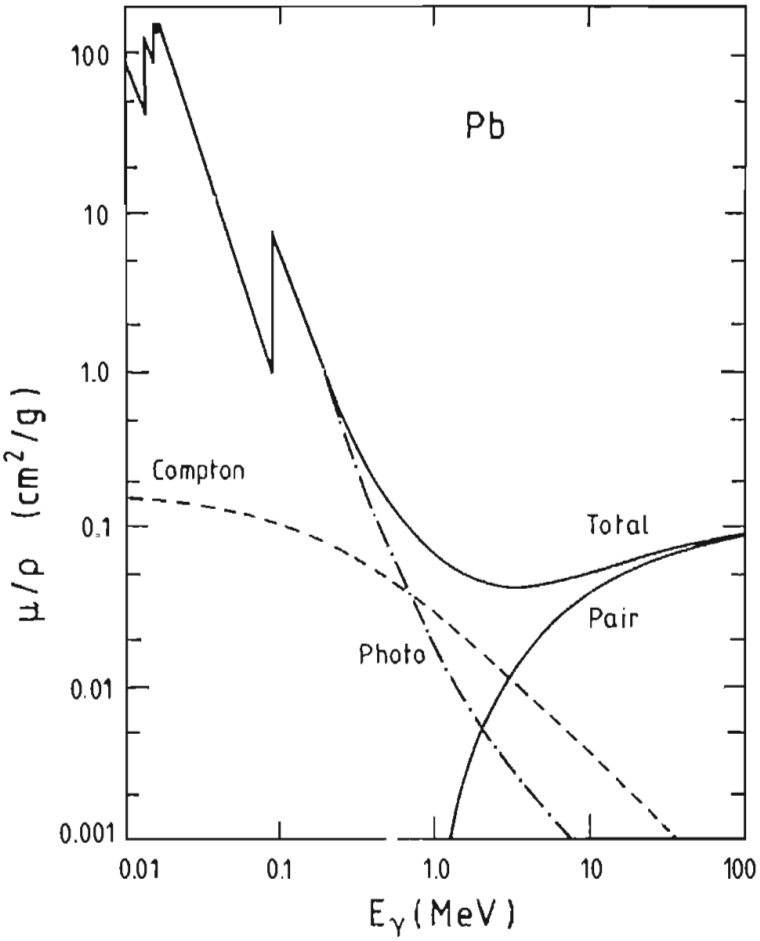

Fig. 2.4. The inverse mean free path, $1/\langle L\rangle\rho$, for photons incident on lead. The distinct physical mechanisms of photoelectric effect, Compton scattering and pair production are evident, along with the 'resonant' behavior near the bound state energies indicated by Eq. 2.6. (From Ref. B.1, with permission.)

energy has $\sigma_{PE}/\sigma_T \sim 6.8\times 10^5$ or $\sigma_{PE}\sim 0.46$ Mb. This estimate from Eq. 2.7 is reasonably close to the value which can be read off from Fig. 1.10.

At photon energies below about 1 MeV in lead the photoelectric effect dominates. Above 1 MeV the Compton effect (relativistic elastic photon scattering), see Chapter 10, then dominates briefly before pair production rises rapidly to be the major physical effect at high energy. At low energies a power law behavior is observed, as expected from Eq. 2.5 which gives a straight line on the log–log plot of Fig. 2.5. The mean free path, $\langle L\rangle\rho$, for photon attenuation is shown, as a function of photon energy, in different materials in Fig. 2.5 for energies from 1 keV to 100 GeV. At high energies the constant value of the pair production cross section is evident as is strong dependence on the atomic number, $\langle L\rangle \sim X_o \sim 1/Z$, where X_o is the radiation length, to be defined later.

At intermediate energies the incoherent nature of the elastic Compton scattering implies that $\langle L\rangle$ is independent of Z, as is seen for photons of 1 to 10 MeV energy.

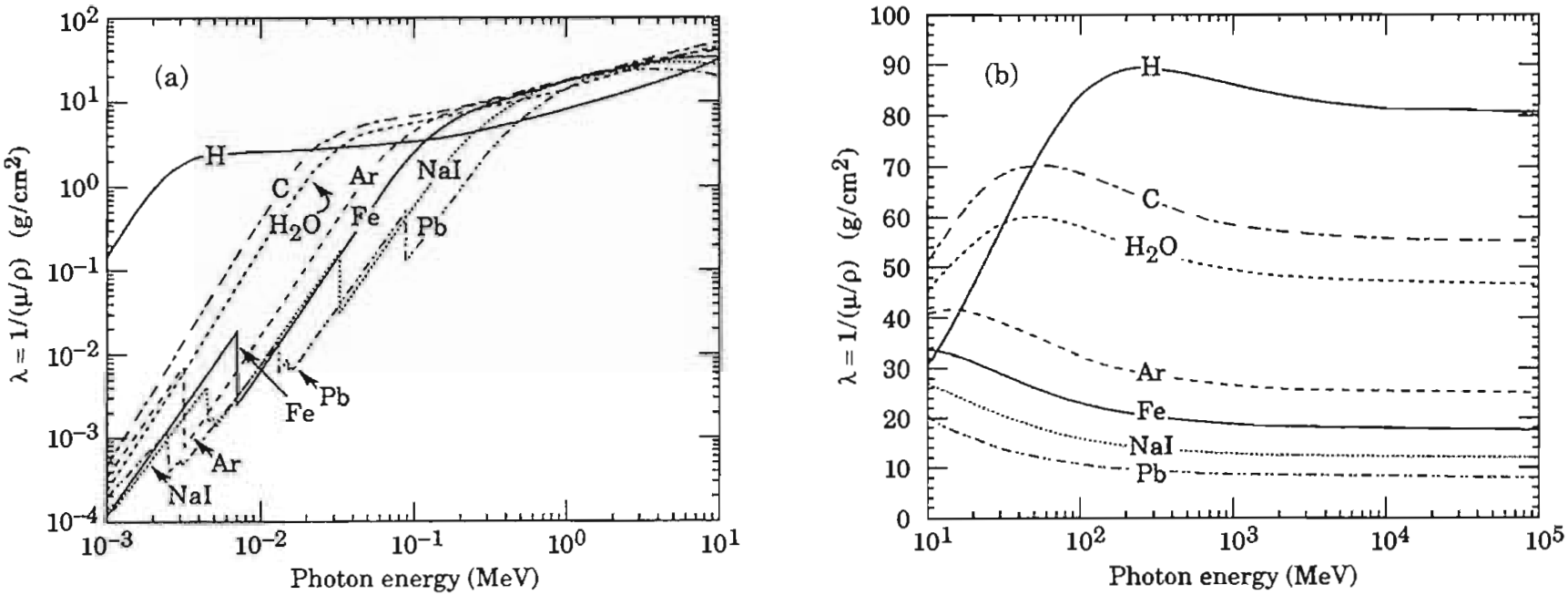

Fig. 2.5. Mean free path, $\langle L \rangle \rho$, as a function of photon energy for different materials. At low energies the photoelectric Z^5 behavior is displayed, while at high energies the energy independent $X_0 \sim 1/Z$ pair production behavior is observed. (From Ref. 1.1.)

At still lower energies where the photoelectric effect is important we see a complicated Z dependence. Looking at Eq. 2.7 we see that the photoelectric cross section goes as Z^5. Clearly the overlap integrals also vary strongly with energy. As an example, picking a photon energy of $\hbar\omega = 10$ keV, we find that the photoelectric cross section in lead is $\sim 2.0 \times 10^5$ barns. The corresponding mean free path is 0.0015 g/cm^2, in reasonable (rough) agreement with the data given in Fig. 2.5.

Note that there are also quantum mechanical effects associated with the emission due to the energy levels shown in Fig. 2.1. As indicated in Appendix B, there is a reflection which can be large. For example, if the potential well of the metal is deep, $U_o = 10$ eV, $E = 0.10$ eV means a reflection coefficient of $R \sim 0.67$ which significantly retards the emission process.

2.3 The angular distribution

The angular distribution of the emitted photoelectron is shown for several photon energies in Fig. 2.6. In the low energy case, $\hbar\omega < mc^2$, there is a classical dipole pattern (see Chapter 10), which can be seen to arise from the $\mathbf{p}\cdot\mathbf{A}$ factor in Eq. 2.3 for $\langle f|A|i\rangle$. The electron is emitted preferentially in the direction of the accelerating transverse electric field of the photon. For high energies, a 'searchlight' pattern (see Chapter 10) develops, $d\sigma/d\Omega < \sin^2\theta/(1-\beta_e\cos\theta)^4$ leading to the electron being thrown forward along the incident photon direction.

2.4 The photomultiplier tube

A major application of the photoelectric effect appears in the photomultiplier tube (PMT). In a PMT use is made of the photoelectric effect to convert a photon signal to an electrical signal where the freed electrons are collected as a current.

As a second application, in Chapter 4 we examine transition radiation detectors which emit x-ray photons. The photoelectric effect is an important source of absorption since this type of detector is not transparent to its own emissions. Thin foils of low Z material are used as radiators which significantly self absorb the emitted x-rays

Let us now turn to photomultiplier tube kinematics. The PMT have special photocathodes which efficiently convert light into electrons. In a solid, the atomic energy level diagram of Fig. 2.1 which is relevant to single atoms becomes more complex. The uppermost populated atomic level is smeared into a continuum (the 'valence band', VB) by the mutual interaction of the electrons

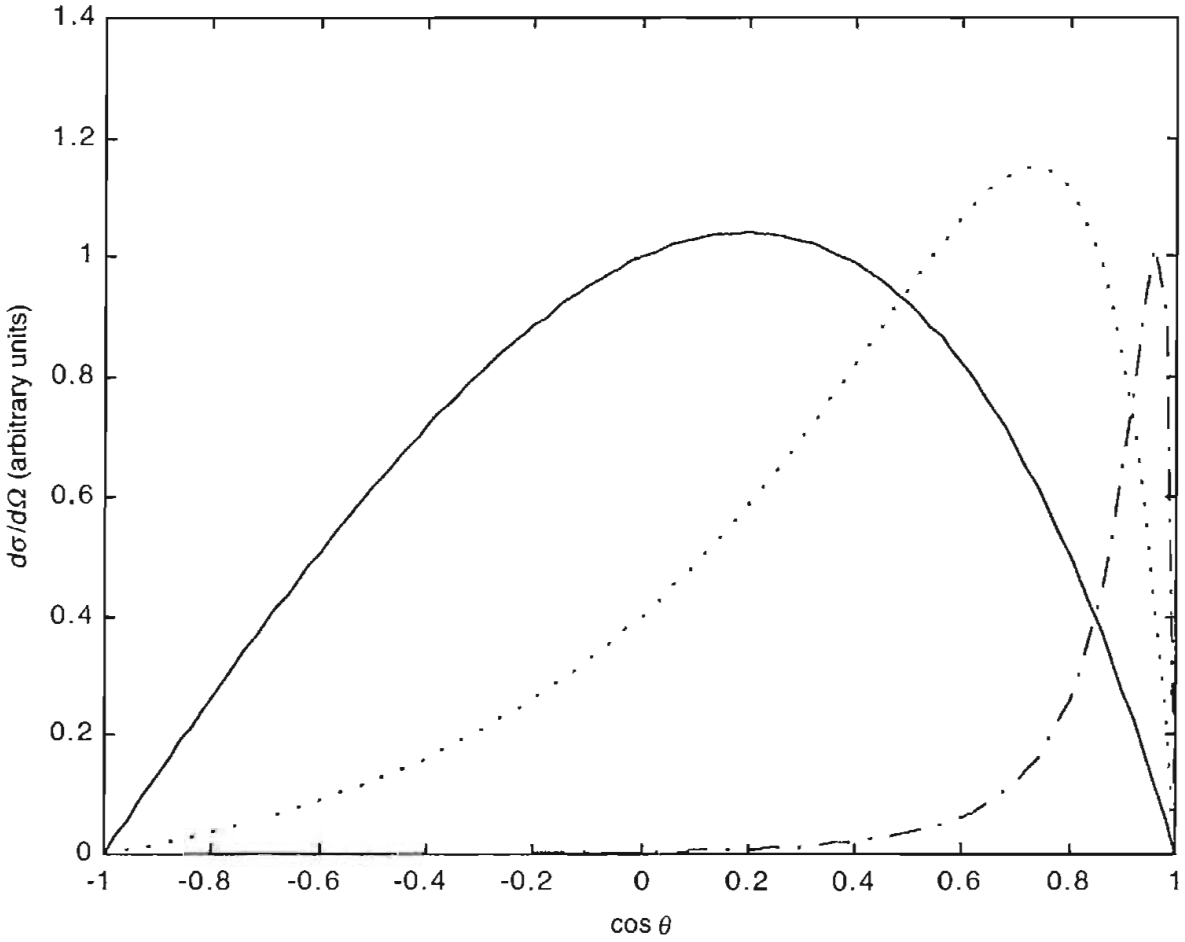

Fig. 2.6. Angular distribution of the photoelectron with respect to the incident photon direction for several recoil electron velocities. —, $\beta=0.1$; · · ·, $\beta=0.5$; –·–·, $\beta=0.9$.

in the solid. The electrons remain bound to the solid. The energy diagram relevant in a metal is shown in Fig. 2.7. Electrons in the metal are bound by energies $\geq eV_{WF}$ (the 'work function'). Absorption of a photon of energy $\hbar\omega$ leads to ionized electrons with kinetic energy T, $T \leq (\hbar\omega - eV_{WF})$. As the reaction time for this process is very short, PMT are very useful devices for the accurate measurement of time.

2.5 Time of flight

A first application of the PMT is the direct measurement of the time of particle passage between two fixed locations. If a system of particles of different masses has been prepared to possess a unique momentum, for example by collimation in a magnetic field (see Chapter 8), then time of flight gives us velocity and hence 'particle identification' or the mass of a given particle. Assume a fixed distance L and a time of passage t. In Eq. 2.8 the relativistic expressions for energy ε and momentum p are used. (See Appendix A.)

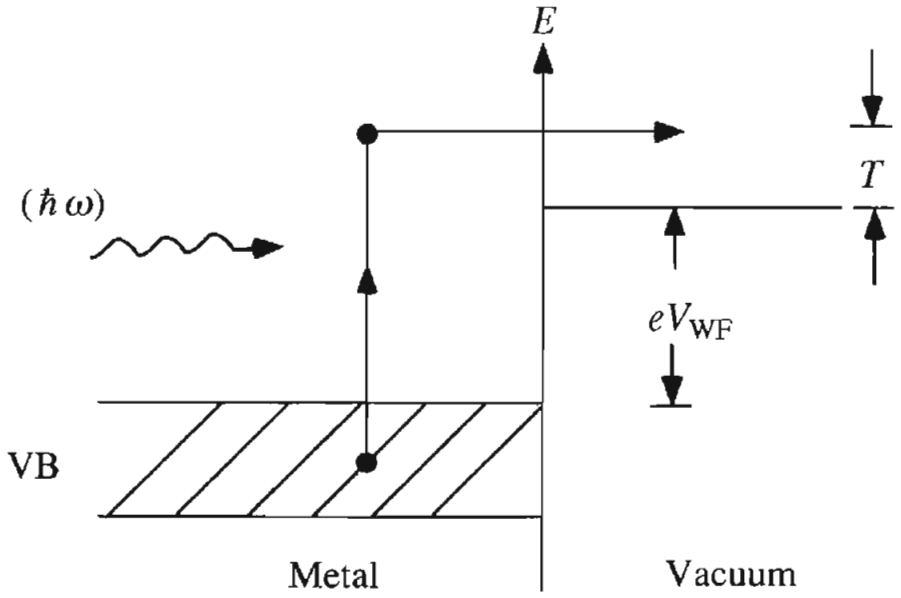

Fig. 2.7. Energy level diagram for a metal.

$$vt = (\beta c)t = L$$

$$\gamma = 1/\sqrt{1-\beta^2} = \varepsilon/m \sim p/m$$

$$\beta = \sqrt{1-\frac{1}{\gamma^2}} \sim 1 - \frac{1}{2\gamma^2}, \quad \beta \to 1 \tag{2.8}$$

$$t \sim \frac{L}{c}\left(1+\frac{1}{2\gamma^2}\right)$$

$$\Delta t \sim \frac{L}{c}\left(\frac{m_1^2 - m_2^2}{2p^2}\right), \quad \beta \to 1$$

For a given flight path, L, the difference in time of flight for particles of different mass, Δt, is proportional to the difference of the squares of the masses of particles. The time separation becomes worse as the inverse of the square of the particle momentum. Therefore time of flight is typically a useful technique only for slow, almost non-relativistic, particles.

The time of flight method collapses at high energies because, by virtue of the special theory of relativity, $\beta \to 1$ independent of the mass. The required flight path at fixed time resolution goes like p^2. For example, to achieve a four standard deviation π/K separation in Δt, $m_\pi \sim 0.14$ GeV, $m_K \sim 0.49$ GeV, with a detector with a resolution of 300 ps, requires a 3 meter flight path, L, at 1 GeV and a 12 meter flight path at 2 GeV. As this example shows, we are normally limited by geometric and fiscal constraints to rather low momenta.

2.6 Scintillators and light collection

So far we have not specified how particle passage is detected and made into a light signal which impinges on the PMT. We now consider the use of plastic 'scintillators' for this purpose. These plastics consist of a 'base' structural plastic which has small additives of 'fluors' dissolved in the base. The real physics of scintillation light production is rather complicated. An incident charged particle first interacts with the atoms of the scintillator exciting a 'primary' fluorescent material which de-excites and emits photons in the ultraviolet. This light is absorbed within a mean free path of ~ 1 mm by a 'secondary' fluorescent material also dissolved in the 'base' plastic which emits in the visible part of the spectrum where the 'base' plastic is fairly transparent.

For example, the primary fluor might be *p*-terphenyl (PTP) which emits at 4400 Å with a 5 ns decay time, while the secondary fluor might be 'POPOP' which emits at 4200 Å in 1.5 ns. A typical base plastic is polystyrene. Suffice it to say that operationally a plastic scintillator emits blue light with a time constant for defluorescence $\lesssim 8$ ns.

Plastic scintillator is a basic workhorse detector used in many applications requiring charged particle detection. The plastic is easy to machine and can be cut and polished into shapes specific to a given application.

A scintillator plus photomultiplier tube system can be used to measure time of flight since all of the components of this system are very fast. Let us work through a typical application. A typical plastic scintillator such as NE102 has a density of about 1 g/cm^3, and an index of refraction n of 1.58. It emits blue light with a characteristic decay time constant of only a few ns.

$$\begin{aligned} \tau &\sim 1.6 \text{ ns} \\ \lambda_{max} &\sim 4250 \text{ Å} (\sim 3.0 \text{ eV}) \end{aligned} \tag{2.9}$$

As a 'rule of thumb' we get roughly one scintillation photon for every 3000 eV of deposited ionization (see Chapter 6) energy (0.1% conversion efficiency). For the case of plastic scintillator, looking in Table 1.2 (see also Chapter 6), this means a yield of about 500 photons per centimeter.

$$\begin{aligned} &1\gamma/3000 \text{ eV} \\ &500\gamma/\text{cm} \end{aligned} \tag{2.10}$$

The emitted light needs to be captured and collected. As it is emitted isotropically inside the plastic, there is a critical angle for total internal reflection, θ_c. In plastic the critical angle is about 39° so that of order $1/3$ of the emitted photons are captured within the plastic and move towards one end. A schematic representation of the capture of the light is shown in Fig. 2.8.

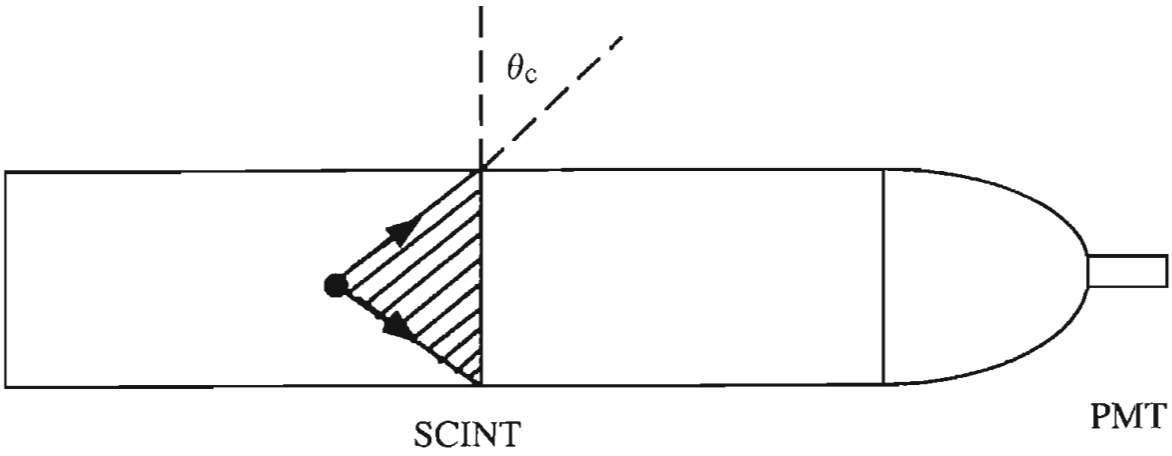

Fig. 2.8. Schematic of a scintillator with phototube readout showing the critical angle for light collection.

$$\sin\theta_c = 1/n$$
$$\theta_c \sim 39^\circ \tag{2.11}$$
$$\frac{\Delta\Omega}{4\pi} = \left(\frac{1-\sin\theta_c}{2}\right) \sim 0.18$$

As a concrete example, a 0.5 cm thick scintillation counter would capture 45 photons within the critical angle. If the optical collection efficiency is only ½ due to poor surface quality of the plastic, we still have 22 photons arriving at the phototube and impinging on the photocathode. The photocathode has some probability to convert the photon into a photoelectron. That probability, the 'quantum efficiency', at the wavelengths emitted by the scintillator may be of order 25%, see Fig. 2.9. We now have 6 photoelectrons coming off the photocathode. Since this is a stochastic or random process, the number of independently emitted photoelectrons is Poisson distributed and the inefficiency, or probability to observe no photoelectrons, at a mean, $\langle N\rangle$, of 6 is 0.2%, i.e. $e^{-6} \approx 0.002$. (See Appendix J.)

$$1-\varepsilon = e^{-\langle N\rangle}, \quad \varepsilon = \text{efficiency} \tag{2.12}$$

A plot of the window transmission coefficient for different PMT as a function of λ is shown in Fig. 2.10. Clearly we can extend the range of photon energies passed by choosing a window made of MgF_2. This ability to pass UV light will be mentioned again in our discussion of Cerenkov counters in Chapter 3. Fiscal constraints may limit us to the use of glass windows which only pass $\lambda > 3000$ Å photons. Since MgF_2 windows are expensive, one other option is to put a layer of 'wavelength shifter' on a cheap glass window. This material

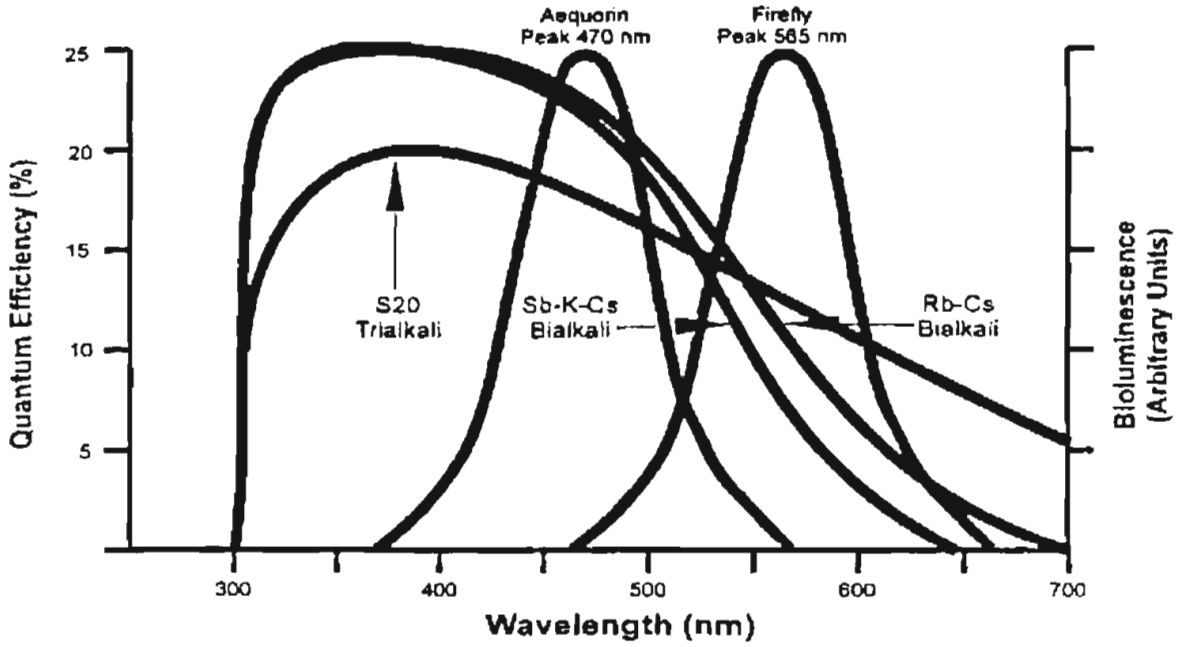

Fig. 2.9. Photocathode 'quantum efficiency' as a function of λ of the light impinging on a PMT. (From Ref. 2.10.)

absorbs high energy photons and re-emits them isotropically at a λ matched to the peak photocathode efficiency. We will see examples of the wavelength shifting (WLS) of light later. Clearly better transmission means more photoelectrons and thus higher detection efficiency.

The photocathode layer is thin because the photoelectric cross section is very large at low photon energies. For typical PMT cathode materials the mean free path for a 1 to 3 eV photon is 10^{-5} cm or 1000 Å. Thus the cathode material may only be about 100 atoms thick and can be vacuum deposited on the glass window. (See Fig. 2.5 and extrapolate in energy as $1/\omega^{7/2}$.)

2.7 Gain and time structure

The rest of the photomultiplier consists of electrodes called 'dynodes'. At each dynode the electrons from the previous stage strike the material after falling through an accelerating voltage. A schematic of a typical PMT electrode structure is shown in Fig. 2.11. Due to secondary electron emission there is electron multiplication by a factor δ, typically of order 3, at each dynode. Therefore, the gain, G, for a tube with 14 dynode 'stages', N_d, is of order 5×10^6. This being a geometric multiplication, the total gain is given by the gain per stage, δ, raised to the power, N_d.

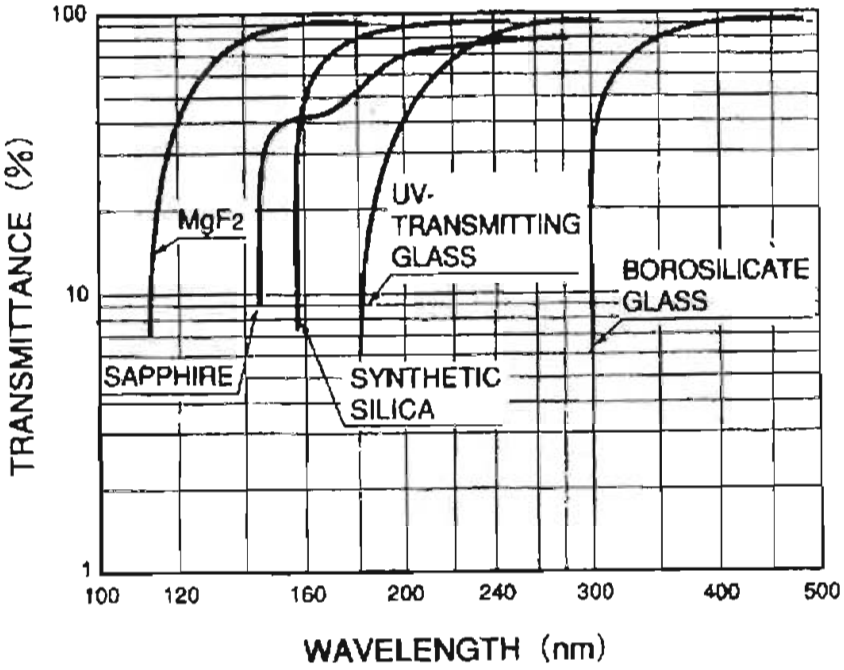

Fig. 2.10. Transmission of different PMT window materials as a function of λ. (From Ref. 2.10.)

$$\delta = \text{gain/dynode} \sim 3$$
$$G = (\delta)^{N_d} = \text{PMT gain} \tag{2.13}$$

Note that the variation in gain with applied voltage, which sets δ, is rapid, which means we need to be careful to regulate the voltage well. Note also that small manufacturing variations in the gain per stage lead to large changes in the overall gain. Thus we expect PMT to have variable gains from tube to tube, which we can equalize by supplying a slightly different voltage to each tube.

For example, the approximate cross section for electron multiplication is given in Eq. 2.14 where I_0 = ionization energy and ε = incident electron energy. For $I_0 = 10$ eV and $\varepsilon = 100$ eV, $\sigma \sim 6.7 \times 10^{-17}$ cm^2 or $\langle L \rangle = 1.7 \times 10^{-7}$ cm in a metal such as copper. Thus the dynodes can be very thin.

$$\sigma(e^- \rightarrow e^- + e^-) < \pi\alpha^2/\varepsilon I_0 \tag{2.14}$$

A contribution to the rise time of the current pulse comes from the spread in kinetic energy of the ejected photoelectrons. The spread is partially caused by the spread of energies in the valence band, as is obvious from looking at Fig. 2.7. Hence there is a spread in transit time to the first dynode, dt. For an initial kinetic energy spread from zero to T, the time spread, dt, for non-relativistic motion in an electric field E is, $dt = \sqrt{2mT}/(eE)$, which for $T = 1.2$ eV in a field of $E = 150$ V/cm is $dt \sim 0.2$ ns.

Yet another contribution to the rise time is the path length difference from

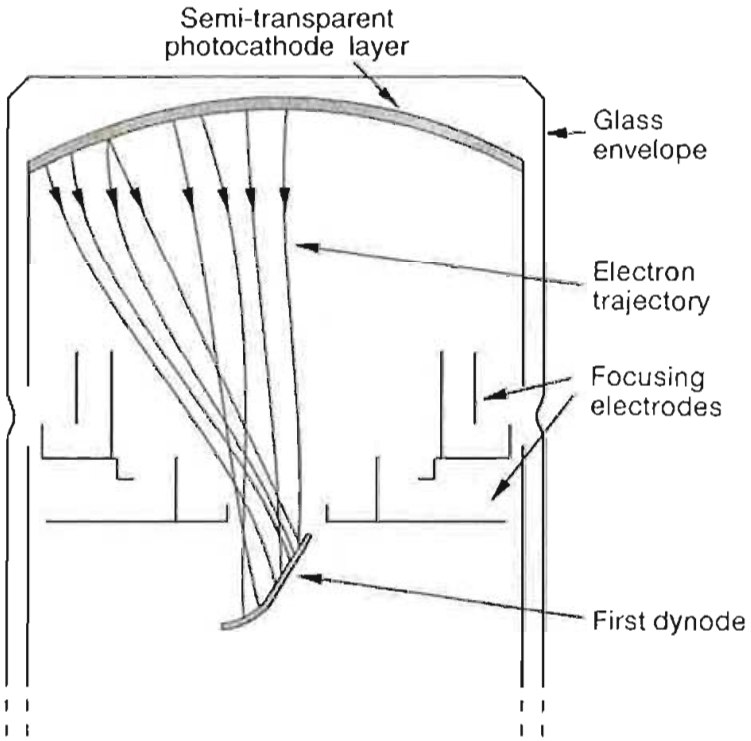

Fig. 2.11. Schematic of the electrode structure of a typical photomultiplier. (From Ref. 2.10.)

the first dynode to different locations on the cathode, as is visible in Fig. 2.11. The resultant spread in arrival times scales with the size of the cathode. Typical values of intrinsic phototube rise time (for 5 cm diameter tubes) are $\sim$2 ns. These times are well matched to the scintillator decay lifetimes. (Eq. 2.9.)

Thus our six photoelectrons, having dropped through a 14 stage tube, become 4.6×10^{-12} C = 4.6 pC of anode signal charge. They are delivered in a rather short time because the photocathode response is effectively instantaneous and the PMT rise time and the fluorescence time of the scintillator are very rapid, $\tau < 3$ ns. If we assume that the total signal charge is delivered in 10 ns, it corresponds to a current of about 0.46 mA. The photomultiplier output is effectively a current source. The PMT current delivered into a standard 50 Ω coaxial cable (see Appendix D) is 23 mV. That level of voltage pulse corresponds to the typical threshold voltages, V_T, which are covered by the fast electronics which are commercially available (see Chapter 2.9).

A photograph of a photomultiplier tube and the resistive voltage divider supplying the multiple dynodes is shown in Fig. 2.12 where we get an idea of the layout of a photomultiplier tube.

An oscilloscope signal trace of the output of a photomultiplier tube driven by a scintillator is shown in Fig. 2.13. Notice that the peak output current is 50 mA and the rise time of the signal is a few ns. This plot serves to illustrate again the order of magnitude of the currents and times which were quoted in

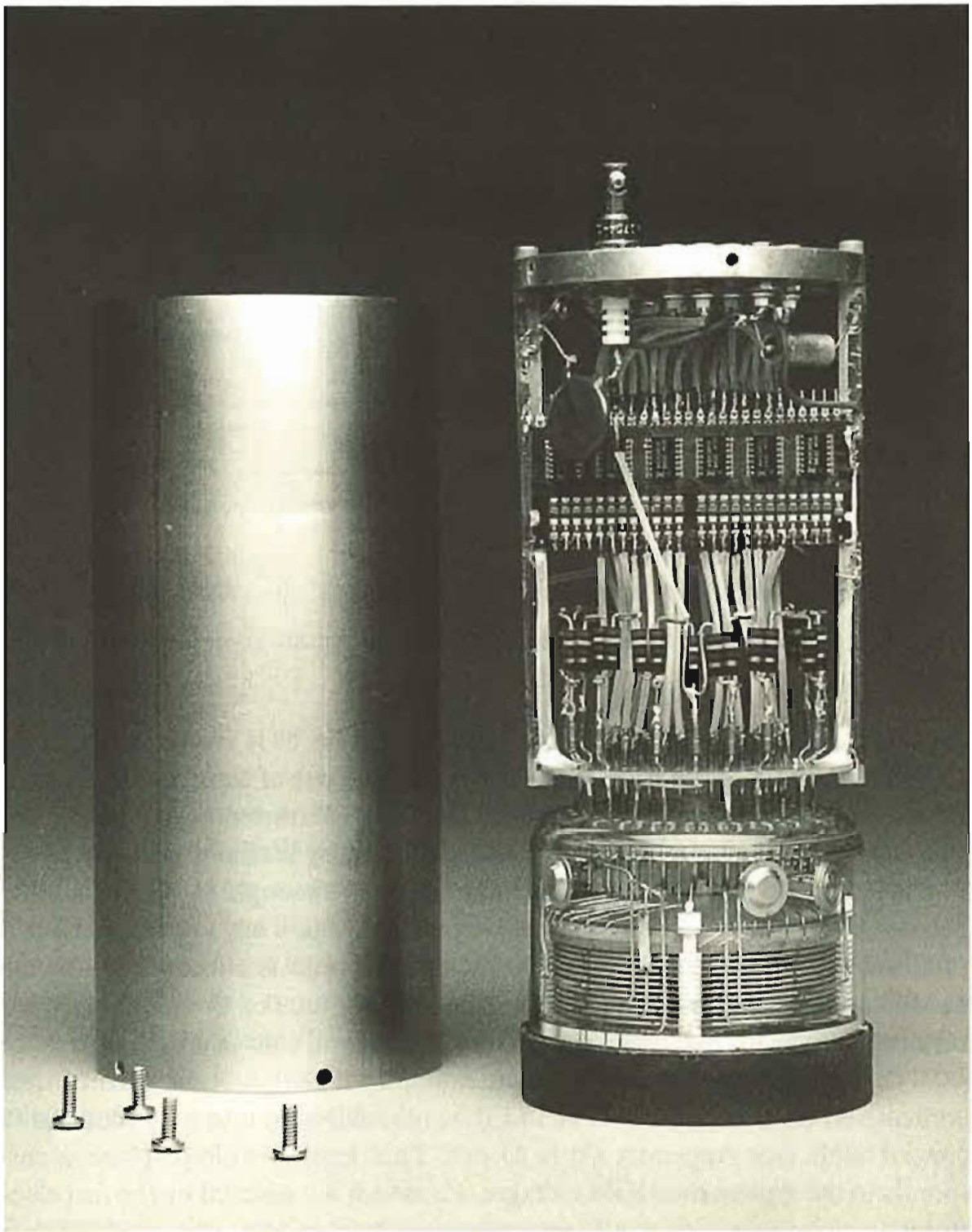

Fig. 2.12. PMT and 'base' assembly showing the dynode structure in the PMT and the system used to supply voltage drop to the successive dynodes. (Photo – Fermilab.)

the numerical example given above. Note that there is a stochastic width to the peak height of the pulse. Its fractional spread is determined by the number of independent primary events or the number of emitted photoelectrons (see Appendix J). For low signal levels we can alternatively look at the fraction of

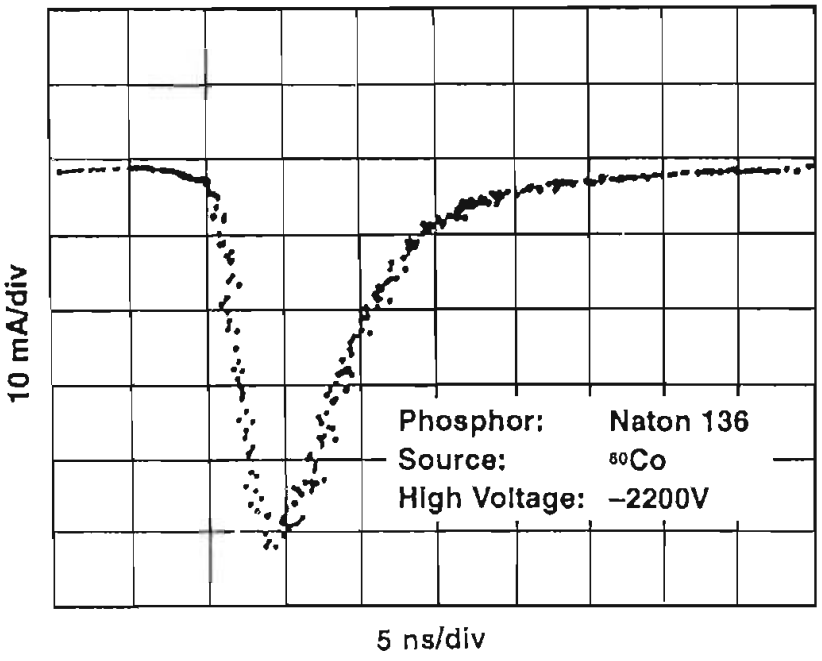

Fig. 2.13. Oscilloscope trace of a PMT current pulse output. Note the rise time of ~ 2 ns and the pulse width of ~ 10 ns full width at half maximum, FWHM. The peak current is ~ 50 mA and the signal pulse height spread is ~ 10%. (From Ref. 2.10.)

time no photoelectrons are emitted and hence, see Eq. 2.12, independently estimate $\langle N_{pe} \rangle$. In Fig. 2.13 the fractional spread is ~ 10% indicating that $\langle N_{pe} \rangle$ is ~ 100, which is 16 times larger than our numerical example.

2.8 Wavelength shifting

There is an interesting alternative solution to the problem of the collection of scintillation light called 'wavelength shifting' (WLS). Typically the Liouville theorem tells us that when we are bringing light out and routing it using total internal reflection to a photomultiplier tube, the 'light pipe' must have an area which does not diminish or we will lose photons. However, these light pipes are unwieldy and ungainly and mean a loss of active detector area because they take up a finite amount of space. The required matching photocathode surface area is also expensive. (See Fig. 2.14a.)

There is a way to evade this difficulty by using a fiber which takes the scintillation light and shifts it to a longer wavelength, captures it by total internal reflection and finally pipes it out to a phototransducer of some sort. Now, at first blush this violates the Liouville theorem. For example, in a typical application one may have a ratio of the primary scintillator area, A, to the secondary

wavelength shifting fiber area, A', which is a factor of order 10^4. (See Fig. 2.14b.)

$$\begin{aligned} A' &\sim \pi a^2 \\ A/A' &\sim 1.3 \times 10^4 \end{aligned} \tag{2.15}$$

The theorem is evaded by red shifting the light. When the light is shifted to longer wavelengths, the energy per photon is reduced and therefore the light is 'cooled'. Since the information content must be the same, we have packed the same information into a smaller area since the information is now 'stored' at lower energies. Thermal noise sets the scale for the smallest allowed storage of information energy. The random thermal energy is defined by the absolute temperature, T, and the Boltzmann constant, k, $\sim kT$. (See Chapter 1.)

The Boltzmann constant, k, is displayed in Table 1.1. As a mnemonic, the Boltzmann constant times the temperature at room temperature, $T \sim 300$ K, is roughly 1/40 eV. Therefore, for example, consider taking light emitted in the blue at about 4500 Å and cooling it to 5000 Å in the green, wavelength shifting by about 500 Å. That 'cooling' corresponds to an energy shift of ~ 0.28 eV.

$$\begin{aligned} \lambda &\sim 4500 \text{ Å} \rightarrow 5000 \text{ Å} \\ \Delta\varepsilon &\sim 0.28 \text{ eV} \end{aligned} \tag{2.16}$$

The increased 'packing factor' by which we can compress the information is given by the exponential of the energy shift, $\Delta\varepsilon$, divided by kT, which defines the theoretical upper limit of information content compression. That ratio is of order 7.3×10^4 in this example, showing that we can achieve very large compression factors. That in turn allows us to make scintillation detectors which are effectively almost fully active since the wavelength shifter fiber uses up only a minuscule fraction of the area of the detector for optical readout. We will return to 'hermetic' detectors in Chapter 12.

$$\begin{aligned} e^{\Delta\varepsilon/kT} &= 7.3 \times 10^4 \\ (kT)_{300\text{ K}} &\sim 1/40 \text{ eV} \end{aligned} \tag{2.17}$$

A picture of the two different kinds of light pipes is given in Fig. 2.14. Figure 2.14a is a photograph of a traditional scintillation assembly with an equal area light pipe. Note how cumbersome the light piping is, even though the equal area law is not even strictly maintained. In contrast, Fig. 2.14b shows a scintillation assembly with wavelength shifter (WLS) readout. It should be clear from the photographs that the ability to cool the information allows for a much more compact and hence 'hermetic' readout.

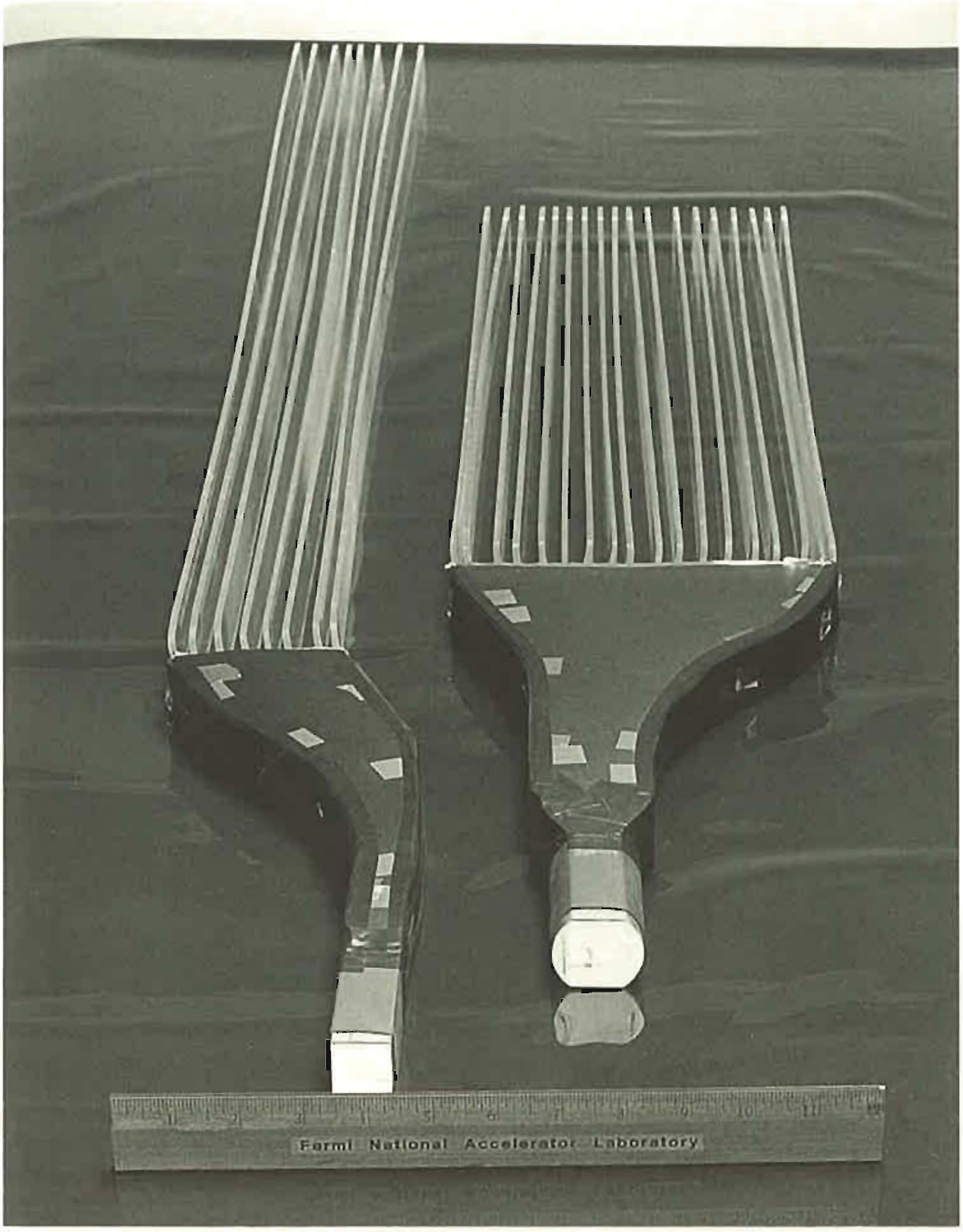

Fig. 2.14a. 'Light pipe' assembly without wavelength shifting. (Photo – Fermilab.)

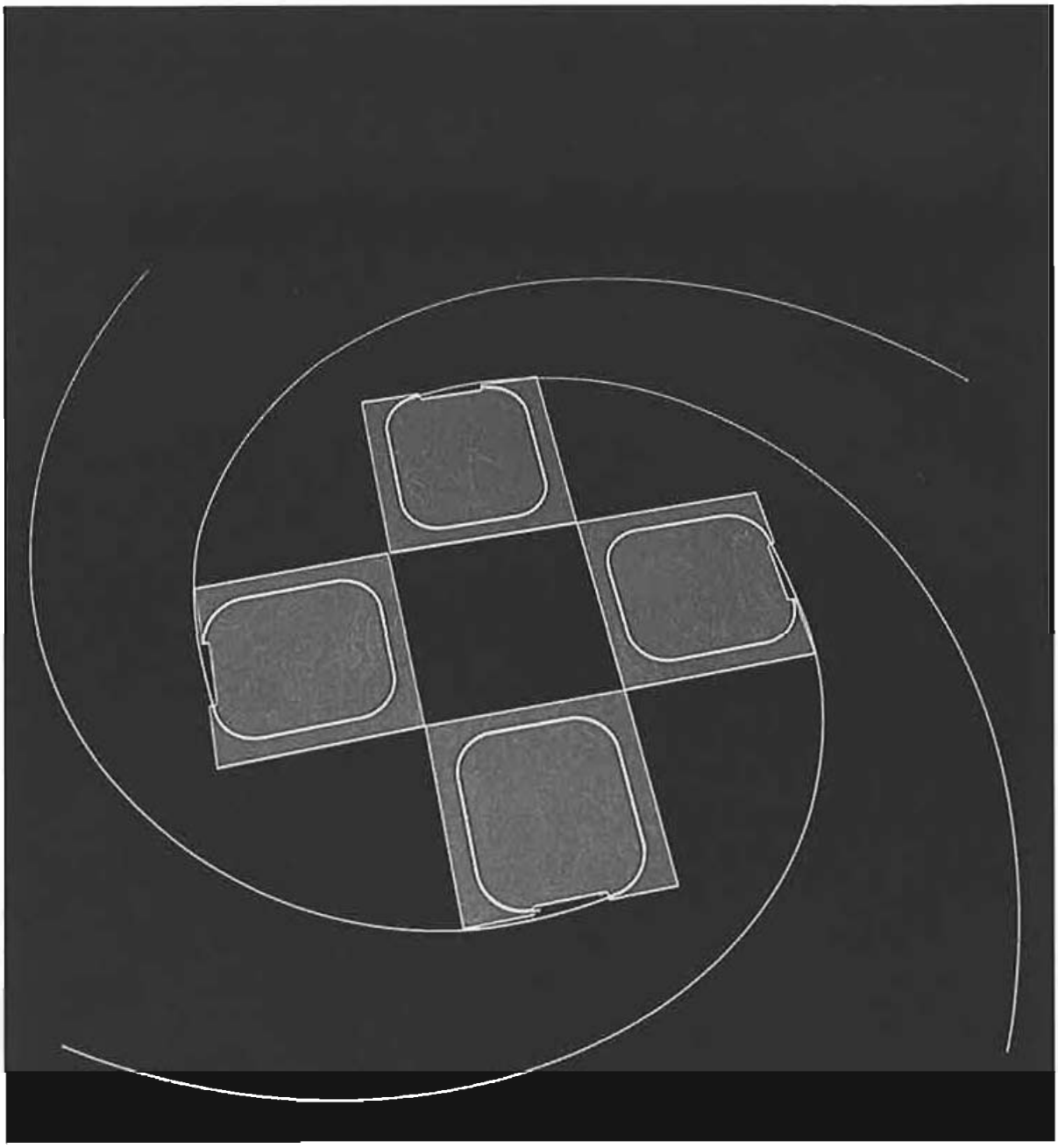

Fig. 2.14b. Array using wavelength shifting fiber. The area ratio of scintillator plate to WLS fiber is $\sim 10^4$. (Photo – Fermilab.)

2.9 Coincidence logic and deadtime

The signals from the anode of a PMT are often used to make logical decisions, i.e. decisions based on Boolean logic. The basis of these decisions is first the initial decision between logical 'ϕ' and logical 'l' and subsequent AND, OR, and NOT electronic operations on the signal. A typical two-fold AND coincidence setup is shown in Fig. 2.15. Signals on inputs 1 and 2 are first 'discriminated' by passing through circuits that give logical 'l' for a fixed time (τ_1 or τ_2) if and only if $V > V_T$ ('threshold' voltage see Appendix I). These signals, C_1 and

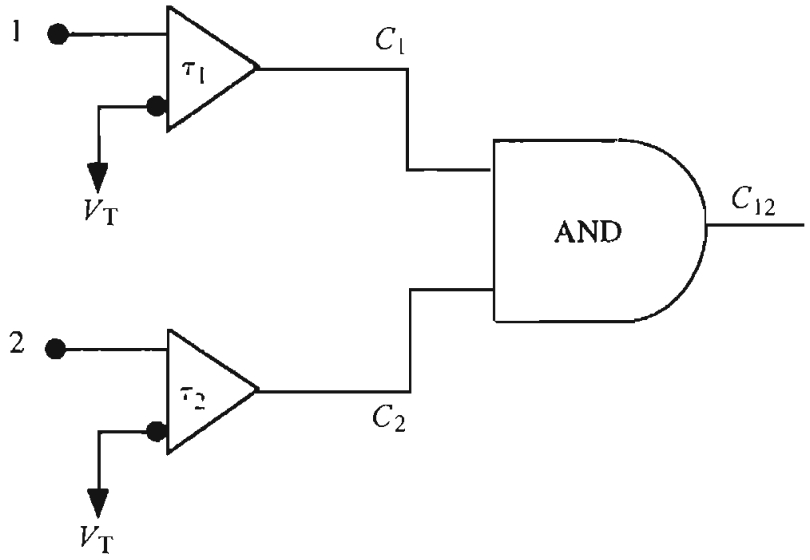

Fig. 2.15. Schematic of a typical discriminator and coincidence logic for a two input AND operation.

C_2, are input to an AND 'gate' which gives a logical '1' output, C_{12}, if and only if both of its inputs are '1', or true, at some point in time (an AND 'coincidence' gate). The method commonly used for most high speed signal connections is to use coaxial cables loaded with a dielectric medium. Although an extremely useful tool, we relegate the discussion of these cables to Appendix D.

Clearly if a particle beam passes through both scintillation counters 1 and 2, the counting rate of the AND gate, C_{12} represents the true particle beam rate. It is also possible that there are false counts due to signals accidentally coinciding in time at the inputs to the AND gate. The timing diagram shown in Fig. 2.16 makes it clear that the time interval appropriate to an accidental two-fold AND coincidence, C_{12}^{A}, is $(\tau_1 + \tau_2)$.

$$C_{12}^{A} = C_1 C_2 (\tau_1 + \tau_2) \tag{2.18}$$

In Eq. 2.18 C_{12}^{A} is the accidental AND rate, C_1 and C_2 are the 'singles rates' and $\tau_1 + \tau_2$ is the 'live time'.

Clearly, a detector with a fast response time is desirable since it makes for a reduced rate of false coincidences. Typically we use logic times, τ_i, which are just sufficient to allow for the intrinsic time 'jitter' of the detector if we are in a high background rate environment. The reason is that this is the shortest live time we can use consistent with full efficiency for real coincidences. Therefore, it yields the minimum accidental rate. An example of one cause of PMT time 'jitter' was shown in Fig. 2.11. Scintillator and PMT logical decisions can be made with live times $\tau \leq 5$ ns, for spatially small scintillators. For example, if $C_1 = C_2 = 1$ MHz, then with $\tau_1 = \tau_2 = 5$ ns the accidental counting rate is $C_{12}^{A} =$ 10 kHz. Digging low rate true signals out of high rate backgrounds often

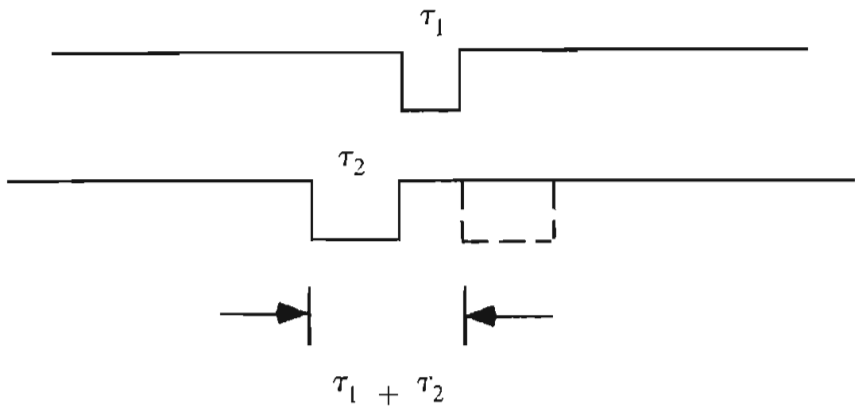

Fig. 2.16. Timing diagram showing a pulse from source 1 of width τ_1 and the range of times for which source 2 of width τ_2 is in accidental coincidence with source 1.

requires a higher level of coincidence, with corresponding lower accidental rate.

Why were photons not seen as quanta prior to the twentieth century? An example of the numerology should help to see why. Suppose you have a 1 W light bulb and you view it with an 'eye' of area 1 mm×1 mm. Assuming a photon of 1 eV, the number of photons entering your eye at a distance of 10 m from this rather dim bulb is still 10^{10} γ/s or 10 photons/ns. Since humans function as millisecond detectors, we perceive the light as a continuous 'fluid'.

In the language of coincidence, with $\tau \sim 10^3$ s, $C\tau$ is $\sim 10^7$, and the eye integrates over millions of photons. As another example the fluorescent lights in your home are flickering on and off at $f = 60$ Hz. Since your eyes integrate due to persistence of vision you are unaware of this behavior and believe you are reading this book under a steady light. Clearly, fast devices are needed to detect the real nature of our environment, and most modern detectors react on the scale of ns.

We close this chapter with a short discussion of the concept of detector 'dead-time'. Suppose we have a detector which is dead to subsequent input signals for a time τ after producing a signal. A typical example would be a Geiger counter which must recharge after a pulse discharges it. Define C' to be the observed output counting rate and C to be the true incident rate. The fraction of time the detector is dead is simply $C'\tau$. Therefore the rate which is lost is

$$\begin{aligned} C - C' &= \text{lost rate} = C(C'\tau) \\ C' &= C/(1 + C\tau) \\ C' &\to 0 \text{ as } \tau \to \infty \\ &\to C \text{ as } \tau \to 0 \end{aligned} \tag{2.19}$$

Clearly, both detectors and electronics with fast pulse recovery, or small dead time τ, are of value in that the observed rate is close to the true rate as long as

$C\tau \ll 1$. For example, if $C = 1$ MHz and $\tau = 5$ ns, then $1 + C\tau = 1.005$ or there is ~a 0.5% loss of signal. The desire to measure the true reaction rate efficiently is why we make particle detectors with short deadtimes.

Exercises

1. Consider a 1 MeV photon incident on a lead atom. Estimate the radius, a, and the ground state energy, ε, of the innermost electron. What is the momentum of the outgoing electron? What is λ_{DB}/a?
2. Estimate the photoelectric cross section using Eq. 2.7 for a 1 MeV photon on lead. Compare to Fig. 1.10 to check your answer.
3. For a particle moving with $\gamma = 5$, evaluate β, $1-\beta$ and the approximation used in Eq. 2.8. Are these approximations good?
4. Find the time of flight difference over a 1 m flight path for pions and kaons with a 1 GeV momentum.
5. How many average detected photons are needed to make a measurement with a 1% inefficiency?
6. You might wonder how to get 100 ps time of flight resolution using PMT with 2 ns rise times. The answer is to have lots of photoelectrons and to have the time resolution defined by the fluctuation on the rise time. How many photoelectrons do you need?
7. Compare the gain of a 6 and a 10 stage tube when the gain per stage is 3.
8. Estimate the 'transit time'of a PMT, the time it takes to go from the photocathode to the anode. Treat the motion as a single drop through a fixed potential, starting at zero kinetic energy. Take a tube distance of 20 cm and a 2000 V potential. Why can we use Newtonian mechanics?
9. Suppose you have two signals which are 5 ns out of time. You want to insert a cable (see Appendices) to put them in time. How many cm of cable do you need to add to the faster signal?
10. Suppose you have two counters with random rates of 100 kHz. The resolving time is 10 ns and the real counting rate is 1000 Hz. What is the accidental rate? Suppose you want an accidental reduced rate. Show that with a third counter, $C_{123} \sim C_1 C_2 C_3 \tau^2$. How much has the accidental rate been reduced?

References

[1] *Quantum Physics*, S. Gasiorowicz, John Wiley & Sons, Inc. (1996).
[2] *Theory and Practice of Scintillation Counting*, J.B. Birks, Pergamon Press (1964).
[3] *Photomultiplier Tubes, Principles and Applications*, Philips Photonics (1995).

[4] *The Art of Electronics*, P. Horowitz and W. Hill, Cambridge University Press (1980).
[5] *Pulse Electronics*, R. Littauer, McGraw-Hill (1965).
[6] R.L. Garwin, *Rev. Sci. Inst.* **31** 1010 (1960).
[7] *Techniques of High Energy Physics*, D.M. Ritson, Wiley Interscience (1961).
[8] *X-Rays in Atomic and Nuclear Physics*, N.A. Dyson, Longmans (1973).
[9] *SCIFI93, Workshop on Scintillating Fiber Detectors*, A.D. Bross, R.C. Ruchti, and M.R. Wayne, World Scientific (1995).
[10] *Photomultipliers and Accessories*, Thorn EMI Electron Tubes (1994).